

Florian A. Mann, Daniel Meyer, Sabrina Mischke and Sebastian Kruss

# CHEMICAL IMAGING WITH NEAR INFRARED FLUORESCENT NANOSENSORS

## 1. INTRODUCTION

Nanomaterials possess optoelectronic properties that are highly interesting both from a fundamental and technological point of view. Due to their new properties and size they can serve as tools to interface and interrogate complex chemical systems such as single cells or even multicellular organisms<sup>[1-3]</sup>. In this article we report on near infrared fluorescent nanosensors with a special focus on carbon nanotube-based sensors. This topic touches different aspects of modern physical chemistry. The near infrared region is highly interesting from a microscopy and spectroscopy point of view. Single-walled carbon nanotubes (SWCNTs) can be imagined as rolled-up graphene sheets and fluoresce in the near infrared (nIR). This rather unique property allows new fundamental investigations in this spectral range and paves the way for promising applications<sup>[4, 5]</sup>.

Furthermore, understanding the mechanism of a fluorescent sensor requires fundamental insights into surface/polymer chemistry, molecular recognition, kinetics and photophysics. Due to their properties SWCNT-based sensors enable completely new approaches in sensing and imaging of complex biological systems.

In this article we discuss new developments in this area (see Fig. 1). First, we will introduce basic properties of carbon nanotubes. After that we will summarize different functionalization and sensing strategies and discuss mechanistic insights into molecular recognition and fluorescence modulation. We will furthermore show how many sensors together can be used for spatiotemporal chemical imaging of target analytes. Finally, we will outline the concept of chemical imaging with fluorescent nanosensors and show the importance of kinetics.

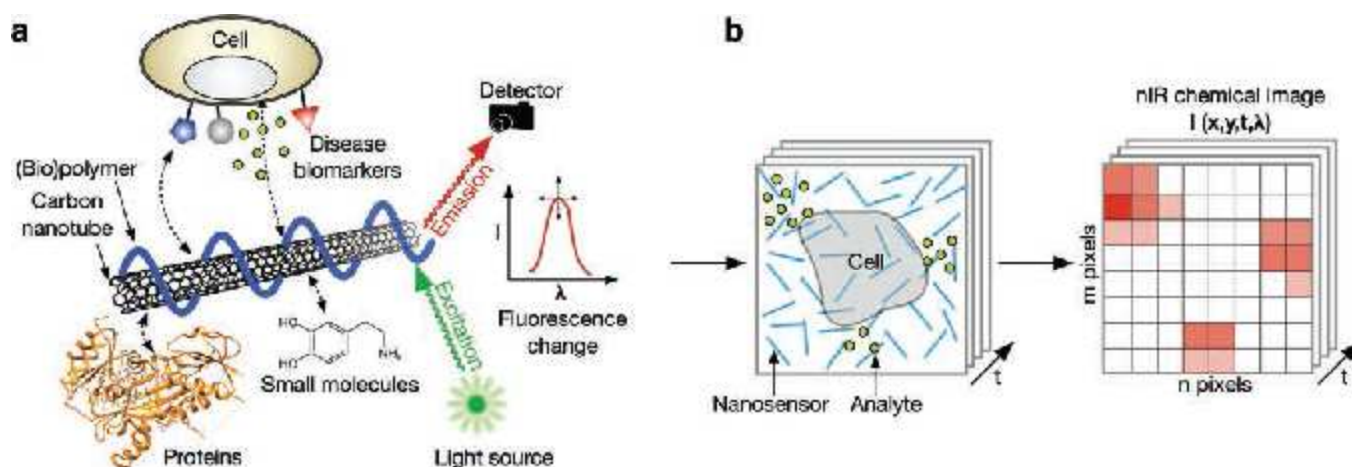


**Fig. 1:** Fluorescent nanosensors for sensing and chemical imaging. a) A fluorescent building block such as a near infrared fluorescent carbon nanotube is decorated with a (bio)polymer, which adsorbs and folds on the hydrophobic SWCNT surface and creates an organic phase (corona). In certain cases, this phase is able to selectively recognize target molecules and change the SWCNT's nIR fluorescence. b) Collective imaging of many nanosensors leads to images that contain information about the local concentration of a substance. One example are sensors immobilized on a surface under a cell that is able to release certain molecules. The corresponding image/movie  $I(x,y,t,\lambda)$  can be interpreted as a chemical image.

M.Sc. Florian Alexander Mann<sup>1</sup>

M.Sc. Daniel Meyer<sup>1</sup>

Sabrina Mischke<sup>1</sup>

Dr. Sebastian Kruss<sup>1,2</sup>

E-Mail: skruss@uni-goettingen.de

<sup>1</sup> Institute of Physical Chemistry, Göttingen University, 37077 Göttingen, Germany

<sup>2</sup> Center for Nanoscale Microscopy and Molecular Physiology of the Brain (CNMPB), Göttingen, Germany

## 2. CARBON NANOTUBES AS BUILDING BLOCKS FOR MOLECULAR SENSORS/PROBES

### 2.1 SINGLE-WALLED CARBON NANOTUBES

Among the different nanomaterials, carbon nanotubes have attracted a lot of interest due to their unique 1D structure and related properties<sup>[5-9]</sup>. In one dimension (perpendicular to their long axis) they appear to be similar to an organic molecule. In

contrast, in the other dimension they resemble a long polymer or solid. As a consequence, scientists with different perspectives and languages such as solid state physicists and organic chemists meet in this space. Carbon nanotubes occur both as multi-walled carbon nanotubes (MWCNT) and as single-walled carbon nanotubes (SWCNT). SWCNTs are cylindrical tubes consisting of only one carbon monolayer and can be seen formally as a rolled-up sheet of graphene (see Fig. 2a). The structure of SWCNTs is usually labeled with the chiral index  $(n,m)$ , which describes how a graphene layer would be rolled-up to create a SWCNT. The chiral index also determines the SWCNT's diameter and its optoelectronic properties (metallic, semimetallic or semiconducting)<sup>[8]</sup>.

Semiconducting SWCNTs are especially interesting for sensor applications. Their bandgap leads to near infrared fluorescence - a striking feature of semiconducting SWCNTs (Fig. 2b)<sup>[10]</sup>. The corresponding emission wavelength varies from approximately 900 nm to 1700 nm and depends on the chiral index (Fig. 2c). SWCNTs are typically excited in the visible range (e.g. the  $S_{22}$  transition at  $\approx 560$  nm for (6,5)-SWCNTs) to gain nIR emission (e.g. the  $S_{11}$  transition at  $\approx 980$  nm for (6,5)-SWCNTs). As a consequence, SWCNT fluorescence is characterized by a large Stokes-shift of more than 400 nm. The longer emission wavelength in the nIR regime leads to less scattering and also reduced background due to autofluorescence (e.g. from proteins) in biological samples<sup>[10]</sup>. SWCNTs do also not bleach<sup>1</sup> and blink<sup>2</sup>, which renders them promising fluorophores for deep-tissue imaging in biomedical applications<sup>[14]</sup>. As a result, single SWCNTs can be observed and studied in (simple) wide-field fluorescence microscopy setups and do not require total internal reflection fluorescence (TIRF) setups as those used for imaging of single organic fluorophores.

<sup>1</sup> The fluorophore loses its fluorescence emission irreversibly due to a chemical reaction.

<sup>2</sup> The fluorescence intensity fluctuates (fluorescence intermittency).

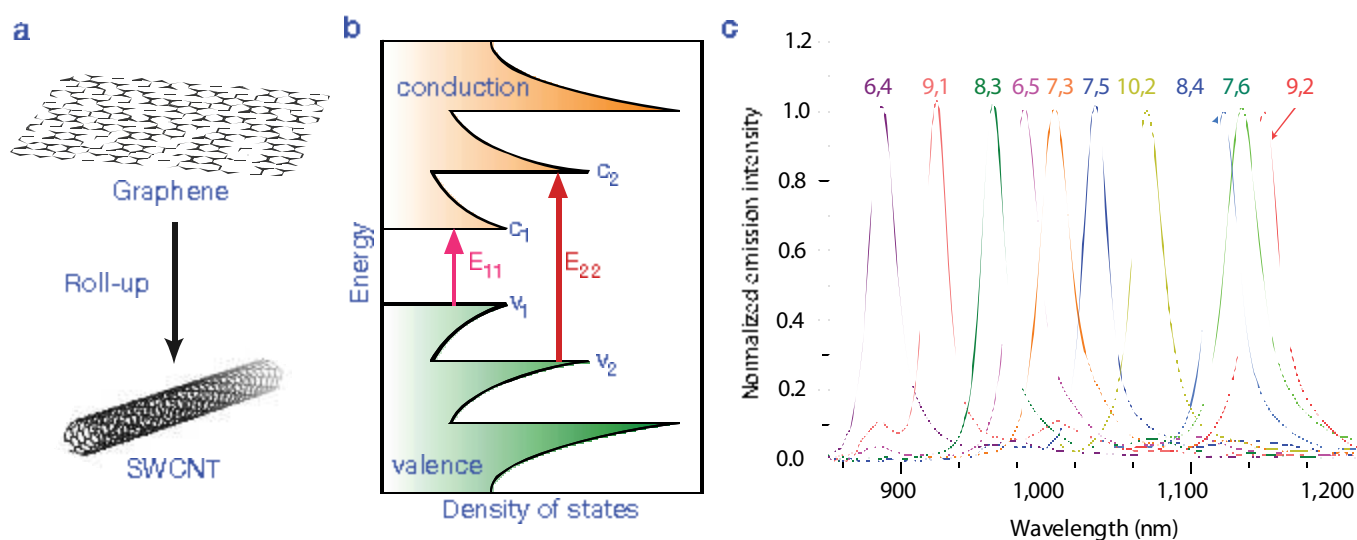


**Fig. 2:** Single-walled carbon nanotubes and their photophysical properties. a) Illustration of the imaginary roll-up of a carbon monolayer (graphene) to create a single-walled carbon nanotubes (SWCNT). b) Density of electronic states diagram of semi-conducting SWCNTs and transitions between van-Hove singularities that lead to chiral index  $(n,m)$  dependent absorbance and fluorescence spectra.  $E_{11}$  and  $E_{22}$  indicate electronic transitions that correspond to optical transitions ( $S_{11}$  and  $S_{22}$ ). c). Fluorescence spectra of carbon nanotubes of different chirality ( $S_{11}$  region). Reproduced and modified with permission from <sup>[5]</sup>, <sup>[12]</sup> and <sup>[13]</sup>.

In contrast to organic fluorophores, fluorescence in SWCNTs is of excitonic nature as proven by 2 photon absorption experiments<sup>[14]</sup>. Excitation moves an electron to the conduction band and leaves a hole in the valence band. This electron-hole pair (exciton) can be interpreted as a quasi-particle and moves along the SWCNT axis until it emits a photon or takes another decay pathway. The binding energy of these excitons is high ( $\approx 400$  meV) and its size was estimated to be on the order of 2 nm<sup>[14, 15]</sup>. During its life time an exciton travels around 100 nm<sup>[16]</sup>. This excitonic nature of SWCNT fluorescence is an advantage from a sensors point of view because an exciton explores its chemical environment when travelling/diffusing along the SWCNT axis<sup>[17, 18]</sup>.

In general, quantum yields (QY) of fluorophores in the near infrared are smaller than those in the visible range<sup>[19]</sup>. The lower fluorescence QY of SWCNTs has been a drawback in the past, but recently bulk QY of 20 % in organic solvents and single SWCNT QY of 30 % in aqueous solutions have been reported<sup>[20, 21]</sup>. The QY depends also critically on sample preparation, which is not yet as evolved as for other nanomaterials. Until recently it was also believed that covalent defects always decrease the fluorescence QY because the exciton would dissipate the energy when it hits the defect. Interestingly, it is becoming more and more evident that certain defects cause a redshifted peak in the nIR fluorescence spectrum, which can dramatically increase the overall QY<sup>[22-24]</sup>. Therefore it is very likely that further advancements in synthesis, purification and defect engineering will lead to higher QYs<sup>[25]</sup>.

Due to all these aforementioned properties SWCNTs have already been used as photostable and nIR-fluorescent labels. Examples are the conjugation of SWCNTs to the therapeutic antibodies Rituximab and Trastuzumab for cancer cell targeting and nIR imaging<sup>[26]</sup>. Furthermore, they have been conjugated to other proteins as calmodulin<sup>[27]</sup> or nucleic acids for DNA hybridization assays and intracellular imaging<sup>[28]</sup>. Another intriguing example is labeling of bacteria by phage functionalized SWCNTs that are able to report bacterial infections *in vivo*<sup>[29]</sup>.

## 2.2 CARBON NANOTUBE-BASED FLUORESCENT SENSORS

As described above SWCNTs provide several desirable photophysical properties, which makes them highly interesting tools for fluorescence-based methods. All atoms of a SWCNT are surface atoms and therefore small perturbations could affect their photophysical properties such as emission wavelength and fluorescence intensity<sup>[30, 22]</sup>.

In contrast to labeling applications, a (molecular) sensor or probe has two additional requirements. First, a sensor requires a selective interaction or binding of the target molecule (recognition unit). Second, the binding event has to be translated into an observable signal such as a fluorescence change (signal transduction). The next sections present examples of different SWCNT-based sensors and are organized according to different molecular recognition concepts.

### 2.2.1 DIRECT DETECTION BY QUENCHING AND DETECTION WITH KNOWN RECOGNITION MOTIFS

The first fluorescent sensors generated with SWCNTs detected reactive oxygen/nitrogen species (ROS/RNS) such as NO, H<sub>2</sub>O<sub>2</sub> or OH-radicals, which play a critical role in many cellular functions including signaling and host defense<sup>[31-33]</sup>. These ROS/RNS most likely adsorb onto the SWCNT surface and quench the fluorescence of SWCNTs and thereby enable quantitative monitoring of cellular H<sub>2</sub>O<sub>2</sub> or NO production in real-time<sup>[5, 30, 34]</sup>. It was shown that SWCNT fluorescence is sensitive to single binding/reaction events and therefore suitable for single molecule studies<sup>[16]</sup>.

In order to detect molecules that do not directly quench SWCNT fluorescence upon adsorption, more sophisticated recognition strategies were necessary. In general, known recognition elements can be attached to the SWCNT surface, which proved to be successful for antibodies, lectins and aptamers<sup>[35-37]</sup>.

This concept was successful to detect sugars on antibodies and disease markers<sup>[35, 36]</sup>. The advantage of this concept is that the intrinsic selectivity and binding strength of the recognition unit (e.g. antibody) to the target molecule are guaranteed. However, signal transduction can be poor because binding is only one necessary condition for a functional sensor. For example, if the recognition unit is too large compared to the target molecule, photophysical changes are very unlikely when the target molecule binds. Size issues with large recognition elements such as antibodies have been limiting the use of similar nanowire field effect-based sensors<sup>[38]</sup>. In this case the Debye length limits sensitivity and the use of such sensors under physiological ion concentrations.

### 2.2.2 NEW RECOGNITION CONCEPTS BASED ON ORGANIC PHASE ENGINEERING WITH (BIO)POLYMERS

Understanding and creating a new recognition unit for molecules is one of the great challenges in chemistry. In order to achieve selective interactions with their chemical environment

SWCNTs can be modified covalently or non-covalently. Covalent modifications have the advantage of generating a well-defined and stable conjugate that can be used for demanding studies for instance as a sensor or label in a complex environment. They can be introduced e.g. at defect sites or at the nanotube's ends via oxidation, halogenation, radical reactions, cycloadditions, click-chemistry or nucleophilic or electrophilic attacks<sup>[39-41]</sup>. While these types of modifications generate defined functional nanotubes, they are known to change the sp<sup>2</sup>-hybridized electronic structure of SWCNTs and therefore destroy/affect their excitonic fluorescence, which is necessary for fluorescent sensing. However, very recently Setaro et al. reported a novel type of covalent modification, which was shown to conserve these fluorescent properties<sup>[42]</sup>. This approach utilizes a new [2+1] cycloaddition, which rebuilds the  $\pi$ -network after ring-opening and formation of a heteromacrocyclic. Raman-peaks corresponding to sp<sup>3</sup>-defects did not increase but these anchors could be used for further functionalization such as attachment of gold-nanoparticles for local field enhancement<sup>[42]</sup>.

Despite this recent success the predominant way to functionalize SWCNT is still non-covalent<sup>[43-46]</sup>. SWCNTs themselves are not water-soluble but non-covalent modification or wrapping with amphiphilic structures (polymers, tensides, nucleic acids, proteins etc.) renders them soluble, increases their colloidal stability and prevents aggregation. Furthermore, this type of modification does not harm the electronic structure of SWCNTs and thereby enables their use as a fluorescent building block. Interestingly, it was found that biopolymer functionalized SWCNTs are sometimes able to recognize and detect molecules<sup>[5, 47]</sup>. This type of molecular recognition relies on the structural confinement of the (bio)polymer on the highly hydrophobic nanotube surface and folding of the (bio)polymer into a 3D structure that is not present in solution. These new structural motifs of the SWCNT-surrounding organic phase (corona) are responsible for molecular recognition, which was therefore termed Corona Phase Molecular Recognition (CoPh-MoRe)<sup>[47, 48]</sup>.

It is easy to understand that the molecular structure around a nanoscale object is in the end responsible for molecular interactions. However, it is much more difficult to create exactly the structural motifs required for a target molecule. Surprisingly, this approach has been shown to be successful for different small molecules including riboflavin, L-thyroxine and estradiol<sup>[48]</sup>.

This approach is also possible for biologically very important target molecules as shown by Kruss et al.<sup>[47]</sup>. They found that certain polymer-wrapped SWCNTs change their fluorescence in the presence of small molecules such as neurotransmitters (Fig. 3a). This interesting behavior was found because they functionalized SWCNTs with different polymers including ssDNA, blockcopolymers and lipids. Interestingly, certain DNA sequences (polymers N1-N13 in Fig. 3b) made SWCNTs sensitive to different molecules. For example, dopamine increased the fluorescence of single nucleic acid-wrapped SWCNTs by more than 400 %. Dopamine is an important neurotransmitter involved in reward control and learning, and the loss of

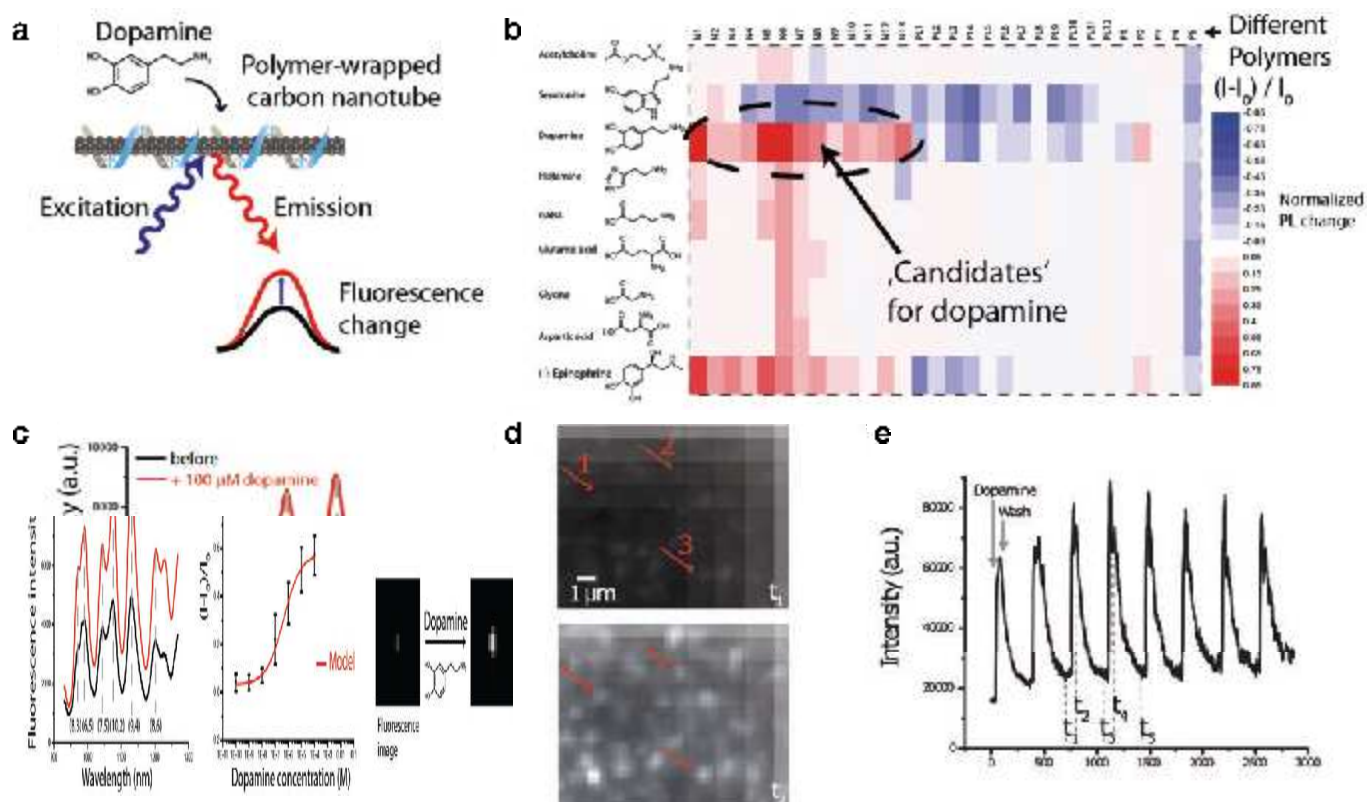


**Fig. 3: Fluorescence responses of (bio)polymer-wrapped single-walled carbon nanotube (SWCNT) to neurotransmitters.** a) Schematic illustration of the concept. A (bio)polymer such as DNA adsorbs onto (wraps around) fluorescent semiconducting SWCNT, which creates an organic phase (corona) around the nanotube that recognizes the analyte and affects the fluorescence spectrum of the nanotube. b) Response map of different SWCNT-(bio)polymer conjugates (x-axis) to different neurotransmitters (y-axis). N1-N13 are DNA/RNA-strands, PL1-PL12 are phospholipids, P1-P5 are amphiphilic polymers. Even though there is cross-reactivity, several promising conjugates can be identified by this screening. c) nIR fluorescence spectrum of SWCNT-(GT)<sub>15</sub>-ssDNA (Polymer N1) before and after addition of dopamine. The different emission peaks correspond to different chiralities (n,m) of SWCNTs present in this sample. d) nIR-fluorescence microscopy images of several SWCNT-(GT)<sub>15</sub>-ssDNA sensors immobilized on a substrate before and after adding dopamine. e) Fluorescence trace of a single dopamine-sensitive SWCNT periodically exposed to 100  $\mu\text{M}$ . Adapted with permission from [47].

dopamine-releasing cells is related to Parkinson's disease<sup>[49]</sup>. Most notably, the fluorescence response depended on DNA-sequence indicating that different sequences cause different sensitivity. It was also possible to show that dopamine detection is reversible (see Fig. 3e). Thus, this class of sensors holds much promise because it enables direct visualization of neurotransmitters (see Fig. 3d). This first dopamine nanosensor had a limit of detection of 11 nM, and dopamine binding was faster than the time resolution of the camera ( $< 100$  ms), which indicates that this type of sensor could meet the specifications for spatiotemporal imaging (see Fig. 1 and section 3). Other related molecules such as L-3,4-dihydroxyphenylalanine (L-DOPA) or homovanillic acid showed much smaller responses than dopamine, which demonstrates a certain selectivity. This is an important finding for the analytical detection of neurotransmitters. While several patch-clamp and electrophysiological methods exist and were recently also transferred to the nanoscale, they are still limited to measuring electrical processes and potentials<sup>[2, 50]</sup>.

This first generation of sensors could not distinguish between very similar catecholamine neurotransmitters such as dopamine and epinephrine. To tackle this problem and further refine sensitivity and selectivity of those sensors Mann et al. investigated a pool of ten different oligonucleotide functionalized

SWCNTs and evaluated their nIR fluorescence responses when exposed to dopamine and its homologues epinephrine and norepinephrine<sup>51</sup>. The authors also collected dose-response curves (Fig. 4a) for the three different neurotransmitters, determined limits of detection and dissociation constants. This approach revealed the dynamic range of the sensors and how they differ in sensitivity especially at realistic lower analyte concentrations. Ultimately the results were used to visualize dopamine in a competitive nIR-fluorescence assay with an equimolar norepinephrine background (Fig. 4b).

A general question is how large the analyte can be to be detected and distinguished by a rather small organic phase. Bisker et al. addressed this question and showed that even large proteins such as fibrinogen can be detected<sup>[52]</sup>. The authors screened a polymer library against several blood serum proteins and thereby found a SWCNT-(bio)polymer sensor for fibrinogen, which was also shown to work in serum at a physiological concentration range. The authors used end-functionalized polyethylene glycols conjugated to phospholipids to functionalize SWCNTs. Fibrinogen decreased the nIR fluorescence intensity of these modified SWCNT. Other proteins caused fluorescence changes as well but with smaller magnitude. This result is striking and opens up great possibilities for future development of nanobiosensors even for larger molecules.

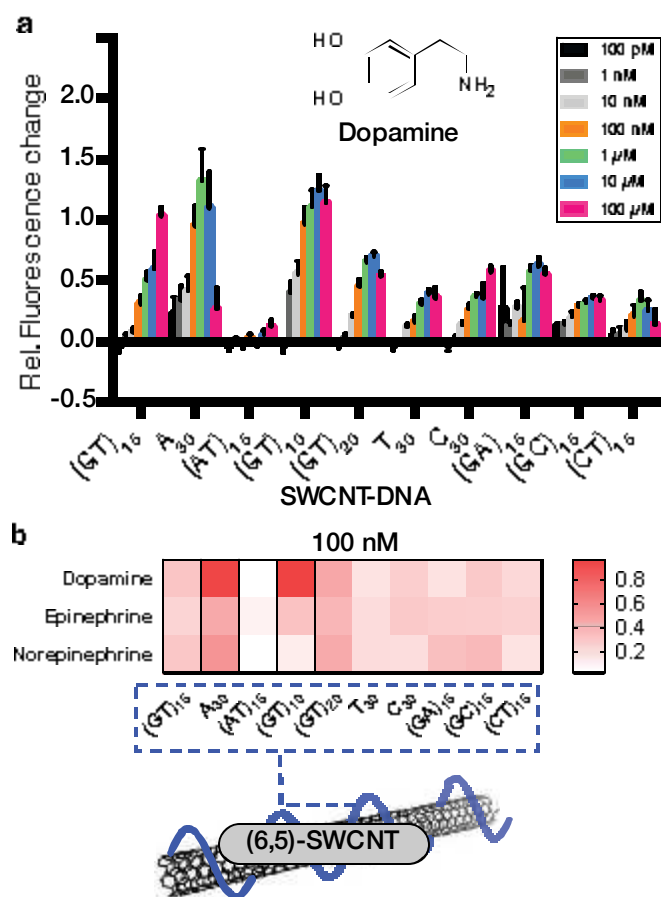


**Fig. 4:** Selectivity and affinity of fluorescent carbon nanotube-based neurotransmitter sensors. a) The most straightforward approach to change the properties of a SWCNT-DNA sensor for neurotransmitters such as dopamine is to change the DNA sequence. Here, dose-response curves for dopamine (epinephrine and norepinephrine not shown) show that most sequences cause a response to dopamine but with different sensitivities. Certain sequences (e.g. (AT)<sub>15</sub>) respond much less to dopamine. b) The differences are much more prominent at lower (realistic) analyte concentrations when most sensors are not yet saturated. Here, the response of SWCNT-DNA sensors to 100 nM of dopamine/epinephrine/norepinephrine was quantified. Reproduced and modified with permission from<sup>[54]</sup>.

### 2.3 INSIGHTS INTO THE MECHANISM OF MOLECULAR RECOGNITION AND PHOTOPHYSICS

To elucidate the mechanism of molecular recognition in the organic phase around carbon nanotubes several studies were performed<sup>[1, 53-55]</sup>. Up to date the example discussed above (dopamine sensitive DNA/SWCNT complexes) is best understood. Apparently, the neurotransmitter dopamine has no influence on the fluorescence of naked SWCNTs (Fig. 5a). In contrast, appropriately DNA functionalized SWCNTs show a strong nIR fluorescence increase, which underlines the importance of the surrounding organic phase<sup>[1]</sup>.

In addition, Kruss et al. performed molecular dynamics (MD) simulations to understand binding between the neurotransmitter and the DNA around the SWCNT<sup>[1]</sup>. These simulations show that dopamine's two hydroxy groups play a crucial role in the recognition event as well as in signal transduction. They first bind to the DNA's phosphate groups and thereby push them closer towards the nanotube surface (Fig. 5c). This reorganization ultimately leads to a change in the local potential. Earlier

it was shown that the DNA sequences showing the weakest sensor response to dopamine display the highest starting fluorescence. Together with this finding, these MD simulations indicate that the movement of the DNA's phosphate groups removes exciton (pre-)quenching sites and thereby leads to fluorescence increase<sup>[1]</sup>.

In another study fluorescence responses to redox-active analytes were investigated<sup>[55]</sup>. Earlier studies had reported that redox-active species affect the fluorescence of SWCNTs<sup>[56, 57]</sup>. Furthermore, spectroelectrochemical studies showed that SWCNT absorption/fluorescence spectra depend on gate voltage<sup>[58]</sup>. Therefore Polo et al. tested the hypothesis that the redox-activity of a small molecule is responsible for fluorescence changes<sup>[55]</sup>. This investigation was very relevant because many small molecules such as dopamine are redox-active. Some reducing molecules, but not all of them, had the tendency to cause fluorescence increases (Fig. 5d). However, the polymer phase around the SWCNTs was the most important factor because analytes of the same redox potential did not show the same responses (see data spread at negative potentials). The fluorescence response was rather modulated by the organic polymer phase (Fig. 5d). Furthermore, it was shown that neither changes in the free surface area, concentration of ROS nor changes in absorption cross section explain the observed intensity shifts<sup>[55]</sup>.

In summary, SWCNTs are an exciting new building block for fluorescent sensors. The first studies showed that fluorescence of SWCNTs is modulated by other molecules and that this modulation depends on the organic phase around the SWCNTs.

However, there are still many aspects not completely understood. First of all, molecular recognition and its relation to signal transduction (photophysics) requires additional experimental and theoretical studies. In general, the structure and dynamics of the phase around nanoscale objects (nanoparticles, proteins) is and remains one of the most fascinating and most difficult topics in physical chemistry.

## 3. CHEMICAL IMAGING WITH NANOSENSORS

### 3.1 IMAGING OF DOPAMINE RELEASE FROM CELLS

The major advantage of optical sensors is their simple integration into sensing schemes with high spatial resolution. Single nanosensors allow the investigation of particular regions of interest. Collective imaging of many nanosensors together even results in a chemical image that contains spatiotemporal information about the analyte concentration (see Fig. 1, Fig. 6a). This kind of information is extremely valuable for biological studies and was validated for dopamine sensitive SWCNT sensors by Kruss et al.<sup>[4]</sup>. The authors used SWCNT-(GA)<sub>15</sub> sensors and densely covered a glass surface to generate a nearly homogeneous surface and maximize signal/noise ratios. This surface array was then used to grow dopamine-releasing pheochromocytoma cells and monitor dopamine release events (Fig. 6a,b).

PC12 cells were stimulated by high potassium levels to release dopamine and the near-infrared image was recorded

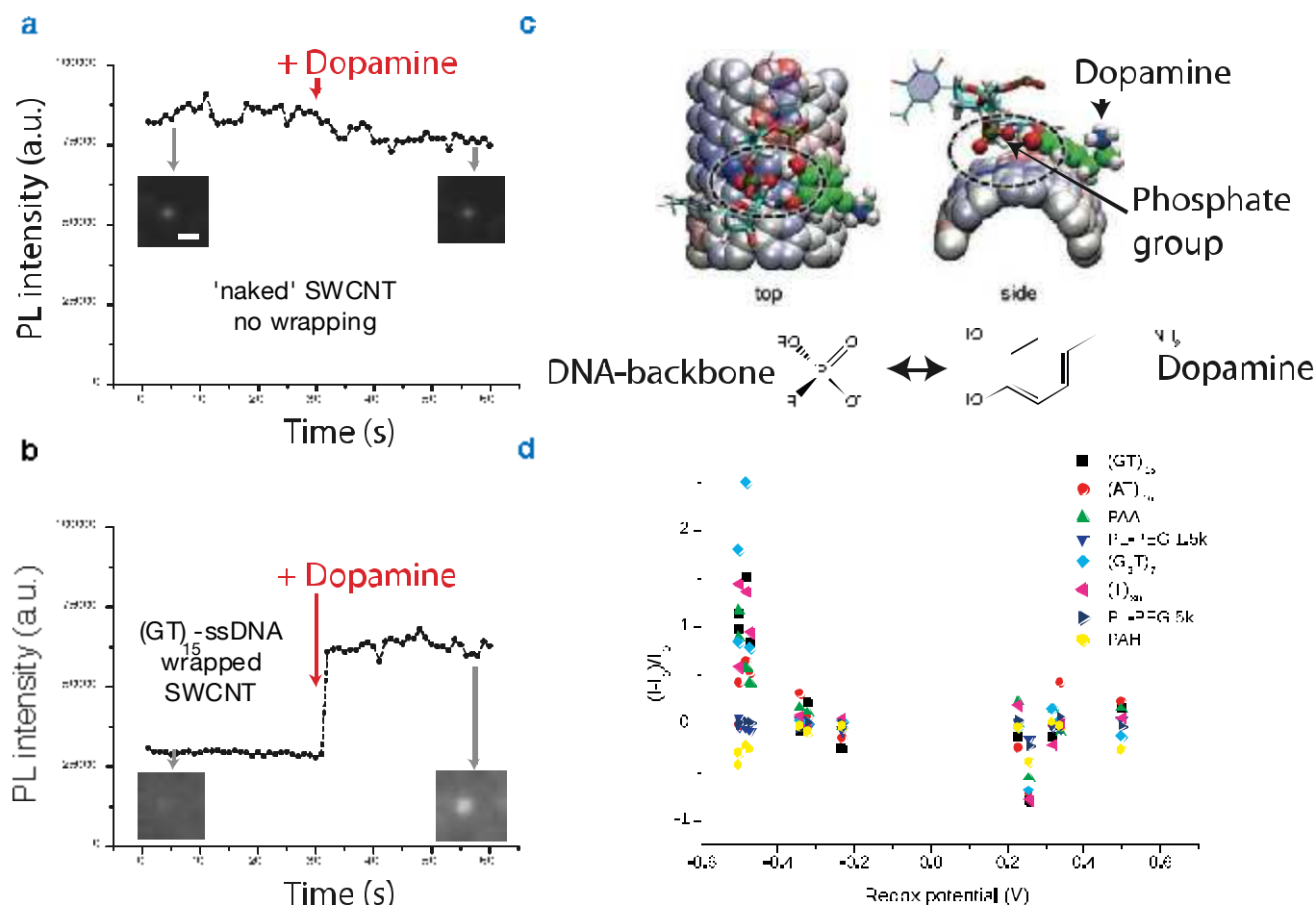


**Fig. 5: Mechanistic insights into fluorescence modulation in carbon nanotube-based fluorescent sensors.** a) Single naked SWCNTs (without functionalization) do not respond to dopamine (1.0  $\mu\text{M}$ ) while (GT)<sub>15</sub>-ssDNA-wrapped SWCNTs increase their fluorescence when dopamine is added (b). c) Molecular Dynamics (MD) simulation of DNA around a nanotube (100 ns). The results indicate that phosphate groups interact with the two hydroxy groups of dopamine. This process changes the potential on the SWCNTs, which most likely affects exciton decay routes. d) Correlation between redox potential and fluorescence response shows larger fluorescence increases for reducing species. On the other side, it depends mainly on the organic phase whether the fluorescence of a functionalized SWCNT gets affected by a molecule and not the redox potential itself (see spread of the data points at -0.5 V). Reproduced and modified with permission from [41] and [55].

with high spatial and temporal resolution. Several frames of the resulting nIR-movie at different time points are shown in Fig. 6d. The false-color images show the fluorescence change (normalized to the starting intensity), which correlates with the dopamine concentration. Before stimulation at time point  $t_0$  only noise could be observed. After stimulation peaks appear and later disappear. These peaks contain information about the dopamine concentration at the given time-point. The high spatial resolution allowed the authors to study directionality of dopamine release and to identify major release sites of dopamine (hotspots). Interestingly, the hotspots were not primarily accumulated at the tips of cellular protrusions but occurred also in regions of negative membrane curvature. In addition, this technique revealed anisotropy of neurotransmitter release from these cells, which is something that could not be measured so far with non-optical methods. The data presented in Fig. 6 is a big step towards chemical imaging with fluorescent nanosensors. In this study only the sensors/pixels below the cell contour could be analyzed due to low signal/noise ratios. In the next step, it would be highly interesting to collect and analyze whole images and maybe observe and quantify dopamine waves diffusing through space. In summary, this imaging technique provides several major

advantages compared to existing techniques especially with respect to spatiotemporal resolution, sensitivity and sensor stability<sup>[41]</sup>. In the future, this approach holds very much promise to study and understand chemical communication in biological systems especially in multicellular systems such as neuronal circuits or biofilms.

### 3.2 KINETIC REQUIREMENTS FOR CHEMICAL IMAGING WITH (FLUORESCENT) NANOSENSORS

Many analytical methods are characterized by thermodynamic equilibrium properties such as dissociation constants and limits of detection. However, if the processes of interest are fast (e.g. release of signaling molecules by cells), the kinetics become highly relevant and it is not trivial to predict the response of a sensor. This consideration is extremely important to quantitatively interpret results. Additionally, rational sensor design requires kinetic insights to circumvent trial and error approaches. For example, a hypothetical sensor with extremely low limits of detection and exquisite selectivity for a signaling molecule could be useless for chemical imaging if it is too slow to capture fast concentration changes.

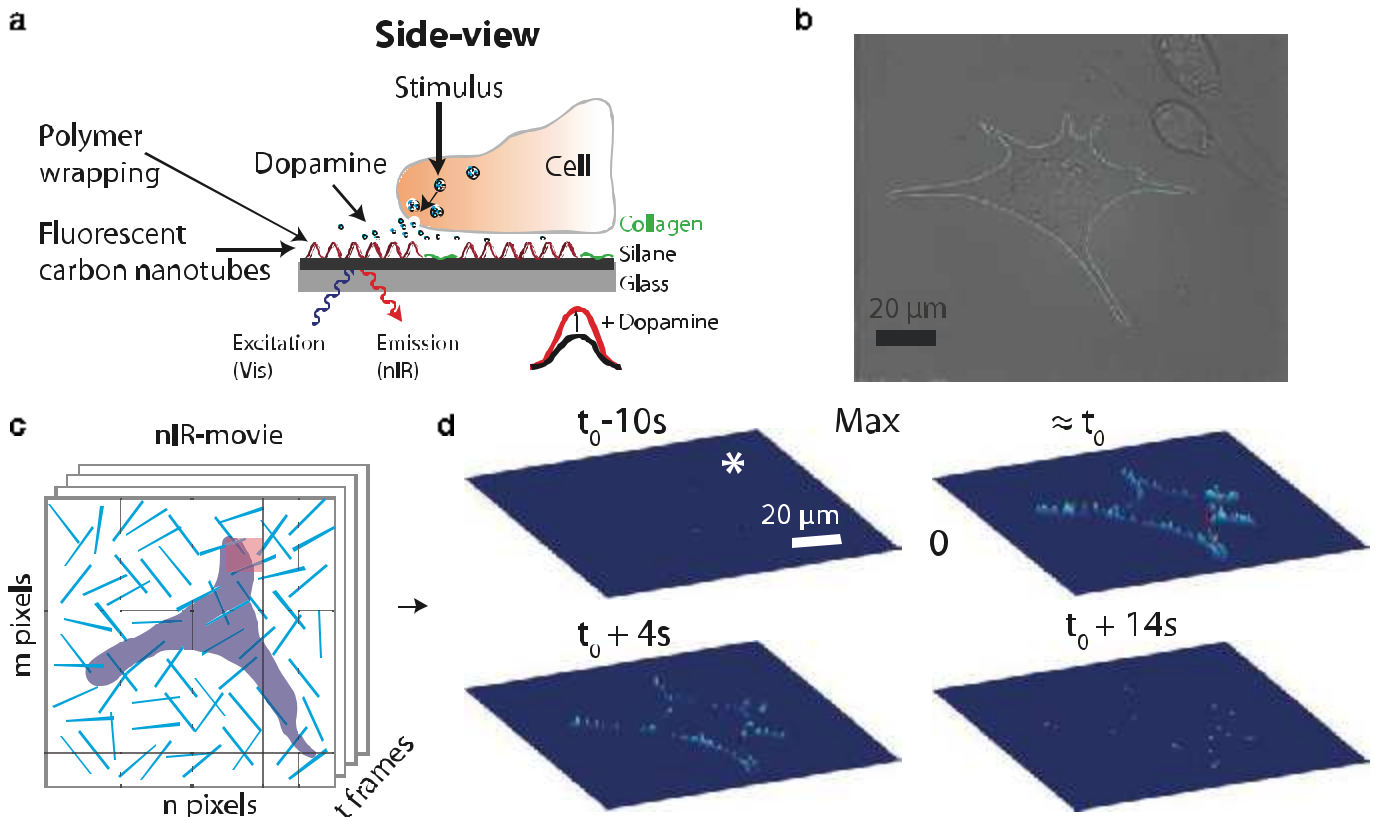


**Fig. 6:** Collective imaging of fluorescent nanosensors to resolve dopamine efflux from cells. **a)** Schematic of the experiment. Dopamine-sensitive SWCNT sensors were attached to a glass surface in a dense layer. Then, cells that are able to release the neurotransmitter dopamine after stimulation were cultivated on top. The nIR fluorescence of a sensor is therefore a local reporter of the dopamine concentration. **b)** Bright field image of a dopamine-releasing PC12 cell. The outline of the cell is shown in blue. **c)** By imaging not only one but many sensors together a chemical image can be observed to monitor the release of dopamine in a spatiotemporal fashion. **d)** The change of the nIR fluorescence in pixels around the cell shown in c (snapshots) shows different stages of dopamine release. Before stimulation at  $t_0$ , only noise can be detected. After stimulation, sensors respond and report about differences in dopamine concentration. Since the sensors are reversible and dopamine is diffusing away, the response decays with time. Adapted with permission from [1].

In this context it is not useful to talk about absolute limits of detection because the temporal and spatial aspect is equally important. To elucidate, what kind of sensitivity and temporal/spatial resolution is required to image release of signaling molecules, Meyer et al. developed a stochastic kinetic simulation that predicts the chemical image of a sensor array (Fig. 7a)<sup>[59]</sup>. This work is important because it conceptualizes chemical imaging with nanosensors and links it to rate constants of sensors. Without this theoretical framework, sensor responses could only be interpreted in a phenomenological way and it remained unclear how sensor kinetics affects data and how an optimal sensor should be designed.

In their new approach, a sensor array was exposed to a concentration profile  $c(x,y,t)$ . In the easiest scenario, cellular release (exocytosis) of a few thousand molecules (e.g. dopamine) and diffusion was simulated (Fig. 7b). Next, the occupation of every single sensor was predicted using a Gillespie-based Monte-Carlo simulation (Fig. 7c). For that purpose, the time until a single analyte binds ( $\tau_{on}$ ) or unbinds ( $\tau_{off}$ ) to or from a nanosensor binding site was calculated by

$$\tau_{on} = \frac{1}{c(x,y,t) \cdot k_{on}} \ln\left(\frac{1}{r_{on}}\right) \text{ and } \tau_{off} = \frac{1}{k_{off}} \ln\left(\frac{1}{r_{off}}\right).$$

Here,  $c(x,y,t)$  defines the concentration around the sensor,  $k_{on}$  and  $k_{off}$  the binding/unbinding rate constants and  $r_{on}$  and  $r_{off}$  represent random numbers between zero and one to simulate stochastic events<sup>[60]</sup>.

Additional aspects such as the Abbe limit and the speed of the detection system (camera) were also taken into account and the response image  $\Delta I(x,y,t)$  is calculated/predicted. The simulation stochastically described all un-/binding processes to binding sites on each sensor. Consequently, occupied binding sites per SWCNT during a certain time  $\Delta t$  could be calculated and translated into a change of sensor intensity. This relative intensity change  $\Delta I(x,y, k_{on}, k_{off}, t)$  reflects how a hypothetical image of the sensors would react to a concentration profile  $c(x,y,t)$  (Fig. 7c). As a result, the generated image series could be analyzed with respect to rate constants to identify what parameters are most relevant.

The authors were able to show that different combinations of rate constants have a dramatic impact on the resulting image (Fig. 7d-g). High values of  $k_{on}$  with slow unbinding rates (Fig. 7g) result in a static response image. The consequence is an over-saturated image and reduced spatial information. Additionally, these sensors could not respond to new release events, which is highly relevant for biological experiments. On the other hand, very fast unbinding rates lead to signals close to the noise level

(Fig. 7d). Thus, nanosensors with appropriate responsiveness in the desired concentration range and the ability to detect and

resolve consecutive events (such as those shown in Fig. 7f) requires tailored binding and unbinding rates.

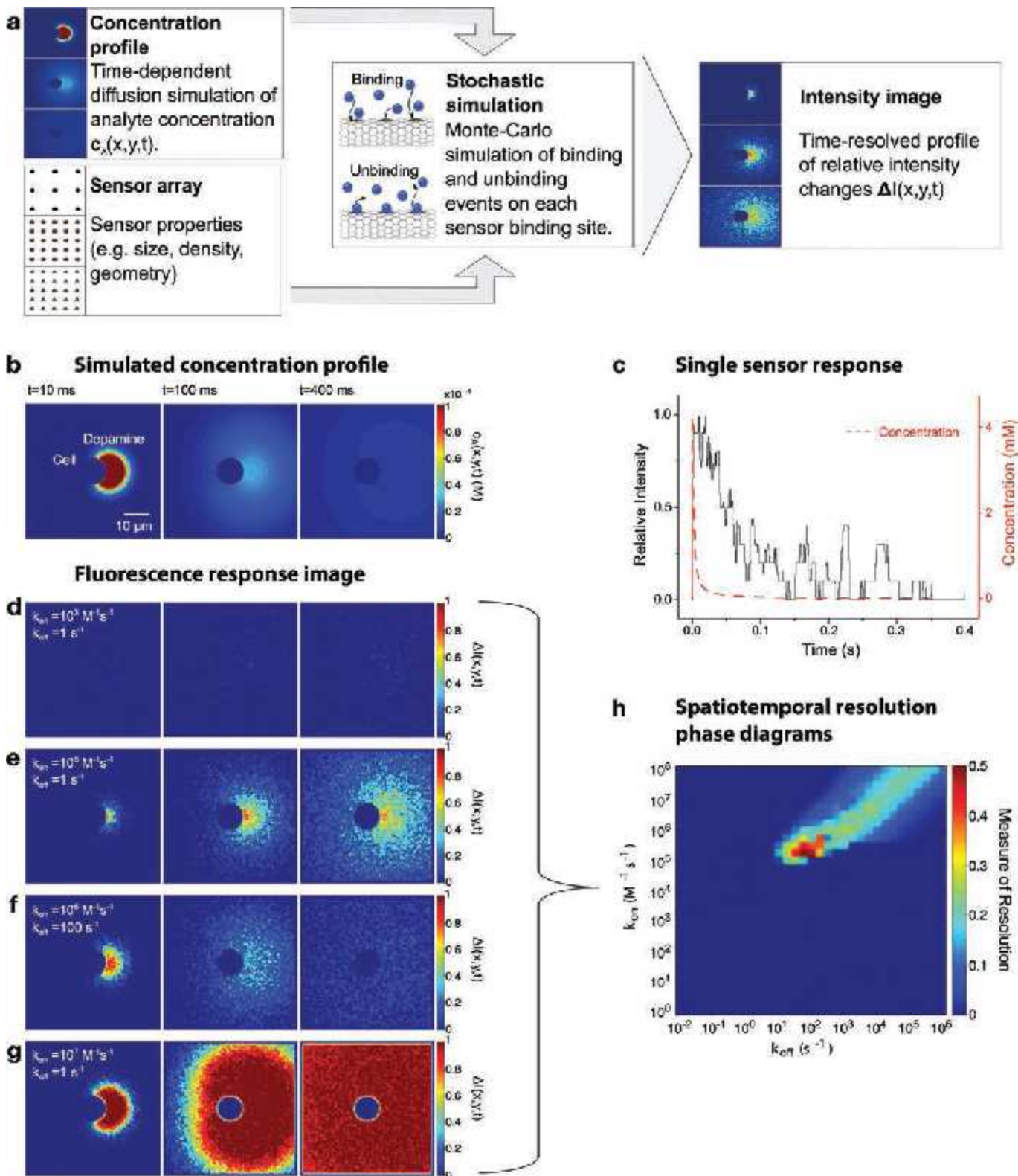


Fig. 7: a) Approach and information flow. A sensor array of a given geometry, density, etc. is exposed to a concentration profile  $c(x,y,t)$  such as the simulated release of neurotransmitters from one vesicle. Binding and unbinding on each nanosensor is simulated using a stochastic kinetic description (Monte-Carlo). Point spread functions of every sensor are overlaid and the image series  $\Delta I(x,y,t)$  is calculated. b) Simulated concentration profile for release of 80000 dopamine molecules from a single cell. c) Concentration (red) and response (black) of a single sensor close to the release point. d-g) Collective response images at different time points at  $t = 10 \text{ ms}$ ,  $t = 100 \text{ ms}$  and  $t = 400 \text{ ms}$  for different reaction rate constants  $k_{on}$  and  $k_{off}$  reveal the strong influence of binding kinetics on the image. h) Phase diagram of the combined spatial and temporal resolution that is achievable for different rate constants. Reproduced and modified with permission from <sup>59</sup>.

By defining measures for resolution the authors were able to simulate phase diagrams (for different rate constants) that allowed them to predict, whether a sensor with given kinetic properties ( $k_{\text{on}}$ ,  $k_{\text{off}}$ ) is able to resolve a certain analytical task (Fig. 7h). In many simulated scenarios  $k_{\text{on}}$  values of  $10^6 \text{ M}^{-1}\text{s}^{-1}$  and  $k_{\text{off}}$  values of  $10^2 \text{ s}^{-1}$  provided the best spatiotemporal resolution, which corresponds to a surprisingly weak dissociation constant  $K_D = k_{\text{off}}/k_{\text{on}} \approx 100 \mu\text{M}$ . These results indicate that lower affinity sensors (corresponding to faster off rates) are better suited for fast chemical imaging, a result that has to be considered in future functionalization concepts.

This theoretical framework is very general and not limited to carbon nanotube-based sensors. It is useful for several reasons. First, it provides insights into the mechanism and predicts resolution limits of chemical imaging with nanosensors. Second, it helps to identify desirable sensor properties and enables rational design instead of trial and error approaches. Third, this simulation helps to interpret experimental data such as those shown in Fig. 6 and might in the future allow at least semi quantitative concentration measurements or comparisons.

#### 4. CONCLUSION

Nanosensors such as those based on fluorescent carbon nanotubes are a rich playground for physical chemistry. Different aspects of surface chemistry and photophysics have to be investigated by spectroscopy and microscopy to gain a mechanistic picture. The unique properties of such sensors and the understanding of their near infrared fluorescence have already paved the way for new applications.

In the future, correlative methods will provide additional insights. For example, the interplay between molecular interactions and optoelectronic properties is still not understood and should be studied in greater detail. Such insights will also enable rational design and synthesis concepts for the organic (macromolecular) phase around nanoparticles and help to tailor sensitivity and selectivity for different bioanalytical tasks. Finally, such sensors can be very useful for a broad range of applications ranging from spatiotemporal imaging of chemical communication in biological systems (systems chemistry) to biomedical diagnostics.

**Acknowledgements:** We thank the Fonds der Chemischen Industrie (FCI), the DFG and the Volkswagen foundation for funding. This project was supported by the state of Lower Saxony (life@nano), the Cluster of Excellence and DFG Research Center Nanoscale Microscopy and Molecular Physiology of the Brain (CNMBP) as well as International Max-Planck Research School (IMPRS) doctoral fellowships to F.A.M. and D.M. We thank Andreas Janshoff and Claudia Steinem and their groups for fruitful discussions and support.

#### REFERENCES

- [1] S. Kruss, D. P. Salem, L. Vuković, B. Lima, E. Vander Ende, E. S. Boyden and M. S. Strano, *Proc. Natl. Acad. Sci. U. S. A.* **114**, 1789-1794 (2017).
- [2] B. Tian, T. Cohen-Karni, Q. Qing, X. Duan, P. Xie and C. M. Lieber, *Science* **329**, 830-834 (2010).
- [3] J. Geng, K. Kim, J. Zhang, A. Escalada, R. Tunuguntla, L. R. Comolli, F. I. Allen, A. V. Shnyrova, K. R. Cho, D. Munoz, Y. M. Wang, C. P. Grigoropoulos, C. M. Ajo-Franklin, V. A. Frolov and A. Noy, *Nature* **514**, 612-615 (2014).
- [4] E. Polo and S. Kruss, *Anal. Bioanal. Chem.* **408**, 2727-2741 (2016).
- [5] S. Kruss, A. J. Hilmer, J. Zhang, N. F. Reuel, B. Mu and M. S. Strano, *Adv. Drug Del. Rev.* **65**, 1933-1950 (2013).
- [6] D. Jariwala, V. K. Sangwan, L. J. Lauhon, T. J. Marks and M. C. Hersam, *Chem. Soc. Rev.* **42**, 2824-2860 (2013).
- [7] V. Georgakilas, J. A. Perman, J. Tucek and R. Zboril, *Chem. Rev.* **115**, 4744-4822 (2015).
- [8] G. Hong, S. Diao, A. L. Antaris and H. Dai, *Chem. Rev.* **115**, 10816-10906 (2015).
- [9] Q. H. Wang, D. O. Bellisario, L. W. Drahushuk, R. M. Jain, S. Kruss, M. P. Landry, S. G. Mahajan, S. F. E. Shimizu, Z. W. Ulissi and M. S. Strano, *Chem. Mater.* **26**, 172-183 (2014).
- [10] M. J. O Connell, S. M. Bachilo, C. B. Huffman, V. C. Moore, M. S. Strano, E. H. Haroz, K. L. Rialon, P. J. Boul, W. H. Noon, C. Kittrell, J. Ma, R. H. Hauge, R. B. Weisman and R. E. Smalley, *Science* **297**, 593-596 (2002).
- [11] O. S. Wolfbeis, *Chem. Soc. Rev.* **44**, 4743-4768 (2015).
- [12] S. M. Bachilo, M. S. Strano, C. Kittrell, R. H. Hauge, R. E. Smalley and R. B. Weisman, *Science* **298**, 2361-2366 (2002).
- [13] S. Ghosh, S. M. Bachilo and R. B. Weisman, *Nat. Nanotechnol.* **5**, 443-450 (2010).
- [14] F. Wang, G. Dukovic, L. E. Brus and T. F. Heinz, *Science* **308**, 838-841 (2005).
- [15] L. Lüer, S. Hoseinkhani, D. Polli, J. Crochet, T. Hertel and G. Lanzani, *Nat. Phys.* **5**, 54-58 (2008).
- [16] L. Cognet, D. A. Tsybolski, J. D. R. Rocha, C. D. Doyle, J. M. Tour and R. B. Weisman, *Science* **316**, 1465-1468 (2007).
- [17] A. G. Walsh, A. N. Vamivakas, Y. Yin, S. B. Cronin, M. S. Unlu, B. B. Goldberg and A. K. Swan, *Nano Lett.* **7**, 1485-1488 (2007).
- [18] T. Hertel, S. Himmelein, T. Ackermann, D. Stich and J. Crochet, *ACS Nano* **4**, 7161-7168 (2010).
- [19] K. Rurack and M. Spieles, *Anal. Chem.* **83**, 1232-1242 (2011).
- [20] A. J. Lee, X. Wang, L. J. Carlson, J. A. Smyder, B. Loesch, X. Tu, M. Zheng and T. D. Krauss, *Nano Lett.* **11**, 1636-1640 (2011).
- [21] S. Y. Ju, W. P. Kopcha and F. Papadimitrakopoulos, *Science* **323**, 1319-1323 (2009).
- [22] S. Ghosh, S. M. Bachilo, R. A. Simonette, K. M. Beckingham and R. B. Weisman, *Science* **330**, 1656-1659 (2010).
- [23] Y. Miyauchi, M. Iwamura, S. Mouri, T. Kawazoe, M. Ohtsu and K. Matsuda, *Nat. Photon.* **7**, 715-719 (2013).
- [24] Y. M. Piao, B. Meany, L. R. Powell, N. Valley, H. Kwon, G. C. Schatz and Y. H. Wang, *Nat. Chem.* **5**, 840-845 (2013).

- [25] I. L. Medintz, H. T. Uyeda, E. R. Goldman and H. Mattoussi, *Nat. Mater.* **4**, 435-446 (2005).
- [26] K. Welsher, Z. Liu, D. Darancioglu and H. Dai, *Nano Lett.* **8**, 586-590 (2008).
- [27] S. H. Yoshimura, S. Khan, S. Ohno, T. Yokogawa, K. Nishikawa, T. Hosoya, H. Maruyama, Y. Nakayama and K. Takeyasu, *Bioconj. Chem.* **23**, 1488-1493 (2012).
- [28] E. S. Hwang, C. F. Cao, S. H. Hong, H. J. Jung, C. Y. Cha, J. B. Choi, Y. J. Kim and S. Baik, *Nanotechnology* **17**, 3442-3445 (2006).
- [29] N. M. Bardhan, D. Ghosh and A. M. Belcher, *Nat. Commun.* **5**, 4918 (2014).
- [30] J. Zhang, A. A. Boghossian, P. W. Barone, A. Rwei, J. H. Kim, D. Lin, D. A. Heller, A. J. Hilmer, N. Nair, N. F. Reuel and M. S. Strano, *J. Am. Chem. Soc.* **133**, 567-581 (2011).
- [31] S. Reuter, S. C. Gupta, M. M. Chaturvedi and B. B. Aggarwal, *Free Radical Biol. Med.* **49**, 1603-1616 (2010).
- [32] M. L. Circu and T. Y. Aw, *Free Radical Biol. Med.* **48**, 749-762 (2010).
- [33] C. C. Winterbourn, *Nat. Chem. Biol.* **4**, 278-286 (2008).
- [34] H. Jin, D. A. Heller, M. Kalbacova, J. H. Kim, J. Zhang, A. A. Boghossian, N. Maheshri and M. S. Strano, *Nat. Nanotechnol.* **5**, 302-309 (2010).
- [35] N. F. Reuel, B. Grassbaugh, S. Kruss, J. Z. Mundy, C. Opel, A. O. Ogunniyi, K. Egoaghe, R. Wahl, B. Helk, J. Zhang, Z. I. Kalcioglu, K. Tvrdy, D. O. Bellisario, B. Mu, S. S. Blake, K. J. Van Vliet, J. C. Love, K. D. Wittrup and M. S. Strano, *ACS Nano* **7**, 7472-7482 (2013).
- [36] J. Zhang, S. Kruss, A. J. Hilmer, S. Shimizu, Z. Schmois, F. De La Cruz, P. W. Barone, N. F. Reuel, D. A. Heller and M. S. Strano, *Adv. Healthcare Mater.* **3**, 412-423 (2014).
- [37] T. G. Cha, B. A. Baker, M. D. Sauffer, J. Salgado, D. Jaroch, J. L. Rickus, D. M. Porterfield and J. H. Choi, *ACS Nano* **5**, 4236-4244 (2011).
- [38] E. Stern, R. Wagner, F. J. Sigworth, R. Breaker, T. M. Fahmy and M. A. Reed, *Nano Lett.* **7**, 3405-3409 (2007).
- [39] A. Hirsch, *Angew. Chem. Int. Ed.* **41**, 1853-1859 (2002).
- [40] M. Prato, K. Kostarelos and A. Bianco, *Acc. Chem. Res.* **41**, 60-68 (2008).
- [41] T. Palacin, H. L. Khanh, B. Jousset, P. Jegou, A. Filoramo, C. Ehli, D. M. Guldi and S. Campidelli, *J. Am. Chem. Soc.* **131**, 15394-15402 (2009).
- [42] A. Setaro, M. Glaeske, D. Przyrembel, T. Bisswanger, G. Gordeev, F. Maschietto, A. Faghani, B. Paulus, M. Weinelt, R. Arenal, M. Adeli, R. Haag and S. Reich, *Nat. Commun.* **8**, 1-7 (2017).
- [43] F. Jakubka, S. P. Schießl, S. Martin, J. M. Englert, F. Hauke, A. Hirsch and J. Zaumseil, *ACS Macro Lett.* **1**, 815-819 (2012).
- [44] C. Backes, F. Hauke and A. Hirsch, *Phys. Status Solidi B* **250**, 2592-2598 (2013).
- [45] A. Di Crescenzo, V. Ettore and A. Fontana, *Beilstein J. Nanotechnol.* **5**, 1675-1690 (2014).
- [46] S. R. Vogel, M. M. Kappes, F. Hennrich and C. Richert, *Chemistry (Easton)* **13**, 1815-1820 (2007).
- [47] S. Kruss, M. P. Landry, E. Vander Ende, B. M. Lima, N. F. Reuel, J. Zhang, J. Nelson, B. Mu, A. Hilmer and M. S. Strano, *J. Am. Chem. Soc.* **136**, 713-724 (2014).
- [48] J. Zhang, M. P. Landry, P. W. Barone, J. H. Kim, S. Lin, Z. W. Ulissi, D. Lin, B. Mu, A. A. Boghossian, A. J. Hilmer, A. Rwei, A. C. Hinckley, S. Kruss, M. A. Shandell, N. Nair, S. Blake, F. Sen, S. Sen, R. G. Croy, D. Li, K. Yum, J. H. Ahn, H. Jin, D. A. Heller, J. M. Essigmann, D. Blankschtein and M. S. Strano, *Nat. Nanotechnol.* **8**, 959-968 (2013).
- [49] R. A. Wise, *Nat. Rev. Neurosci.* **5**, 483-494 (2004).
- [50] J. T. Robinson, M. Jorgolli, A. K. Shalek, M. H. Yoon, R. S. Gertner and H. Park, *Nat. Nanotechnol.* **7**, 180-184 (2012).
- [51] F. Mann, N. Herrmann, D. Meyer and S. Kruss, *Sensors* **17**, 1521 (2017).
- [52] G. Bisker, J. Dong, H. D. Park, N. M. Iverson, J. Ahn, J. T. Nelson, M. P. Landry, S. Kruss and M. S. Strano, *Nat. Commun.* **7**, 10241 (2016).
- [53] G. Bisker, J. Ahn, S. Kruss, Z. W. Ulissi, D. P. Salem and M. S. Strano, *J. Phys. Chem. C* **119**, 13876-13886 (2015).
- [54] D. P. Salem, M. P. Landry, G. Bisker, J. Ahn, S. Kruss and M. S. Strano, *Carbon* **97**, 147-153 (2016).
- [55] E. Polo and S. Kruss, *J. Phys. Chem. C* **120**, 3061-3070 (2016).
- [56] N. V. Kumosov, V. S. Leontiev, A. S. Linnik, O. S. Lytvyn and V. A. Karachevtsev, *Chem. Phys.* **438**, 23-30 (2014).
- [57] A. J. Lee, X. Y. Wang, L. J. Carlson, J. A. Smyder, B. Loesch, X. M. Tu, M. Zheng and T. D. Krauss, *Nano Lett.* **11**, 1636-1640 (2011).
- [58] H. Hartleb, F. Spath and T. Hertel, *ACS Nano* **9**, 10461-10470 (2015).
- [59] D. Meyer, A. Hagemann and S. Kruss, *ACS Nano* **11**, 4017-4027 (2017).
- [60] D. T. Gillespie, *Annu. Rev. Phys. Chem.* **58**, 35-55 (2007).